Giant resonant enhancement of optical binding of dielectric particles

Evgeny N. Bulgakov, Konstantin N. Pichugin, and Almas F. Sadreev
Kirensky Institute of Physics, Federal Research Center KSC SB RAS, 660036 Krasnoyarsk, Russia

(Received 17 June 2020; accepted 11 September 2020; published 20 October 2020)

Optical coupling of two identical dielectric particles gives rise to bonding and antibonding resonances. The latter is featured by significant narrowing of the resonant width and strong enhancement of the Q factor for the high-index micron-size particles in subwavelength range. We consider particles shaped as spheres and disks under coaxial illumination of dual incoherent counterpropagating Bessel beams. In the case of spheres we derive analytical expressions for the optical binding (OB) force which decays and displays two periods of oscillations. For close distances the OB force enormously increases in the resonant regime. The case of two coaxial disks is featured by extremal enhancement of the Q factor owing to the twofold variation over the distance between disks and the aspect ratio of each disk compared to the case of two spheres. In that case we demonstrate enhancement of the OB force up to several tens of nanonewtons. We show that the magnitude and sign of the OB force strongly depend on the longitudinal wave vector of the Bessel beams.

DOI: 10.1103/PhysRevA.102.043518

I. INTRODUCTION

The response of a microscopic dielectric object to a light field can profoundly affect its motion. A classical example of this influence is an optical trap, which can hold a particle in a tightly focused light beam [1]. When two or more particles are present, the multiple scattering between the objects can, under certain conditions, lead to optically bound states. This peculiar manifestation of optical forces is often referred to as optical binding (OB). It was first considered by Thirunamachandran [2] (see also Refs. [3,4]) and observed by Burns *et al.* in 1989 in a system of two plastic spheres in water [5]. This peculiar manifestation of optical forces is often referred to as optical binding (OB) forces. The OB belongs to an interesting type of mechanical light-matter interaction between particles at microscale mediated by the light scattered by illuminated particles. Depending on particle separation, the OB leads to attractive or repulsive forces between the particles and, thus, contributes to the formation of stable configurations of particles. The phenomenon of OB can be realized, for example, in dual counterpropagating beam configurations [6–12]. Equilibrium positions of particles are created by a very weak balance between the optical forces from the incident fields and from the scattered fields generated by the particles. Many researchers have analyzed OB force quantitatively in theory. Chaumet and Nieto-Vesperinas [13] and Ng *et al.* [14] calculated the OB force under illumination of two counterpropagating plane waves. Čižmár *et al.* [15] presented the first theoretical and experimental study of dielectric submicron particle behavior and their binding in an optical field generated by the interference of two counterpropagating Bessel beams. Also, Thanopulos *et al.* [12,16] numerically evaluated the OB force as a function of distance between spheres and frequency.

It is clear that excitation of the resonant modes with high-Q factor in dielectric structures results in large enhancement of near electromagnetic (EM) fields and respectively in extremely large EM forces proportional to squared EM fields. First, sharp features in the force spectrum, causing mutual attraction or repulsion between successive photonic crystal layers of dielectric spheres under the illumination of a plane wave has been shown by Antonoyiannakis and Pendry [17]. Because of the periodicity of the structure, each layer is specified by extremely narrow resonances which transform into the bonding and antiboding resonances for close approaching of the layers. The normal force acting on each layer as well as the total force acting on both layers including the optical binding force follow these resonances. The lower frequency bonding resonance forces push the two layers together and the higher frequency antibonding resonance pulls them apart. Later these disclosures were reported for coupled photonic crystal slabs [18] and two planar dielectric photonic metamaterials [19] due to the existence of resonant states with infinite Q factor (bound states in the continuum).

However, in practice we have arrays of a finite number of dielectric particles which nevertheless show the Q factor exceeding the Q factor of an individual particle by many orders in magnitude [20–22] where the Q factor of the resonant state is given by the ratio of real and imaginary parts of complex resonant eigenfrequency. What is remarkable is that even two particles can demonstrate extremely high-Q resonant modes owing to avoided crossings. The vivid example is avoided crossing of whispering-gallery modes (WGMs) in coupled microresonators which results in an extremely high-Q factor [23,24]. As a result, an enhancement of the OB force of around hundreds of nanonewtons between coupled WGM spherical resonators takes place in an applied power of 1 mW [23]. However, the WGM modes with extremely high orbital momenta can be excited only in spheres with large radii of order 30 μm. Recently we offered a solution to the problem of a large Q factor in the subwavelength regime by the use of two coaxial silicon disks of micron sizes. Owing to twofold

(over the aspect ratio and distance between disks) avoided crossing of low-order resonances, the antibonding resonant mode acquires a morphology of the higher order Mie resonant mode of effective sphere with extremely small resonant width. A comprehensive and detailed description of this phenomenon is given in Ref. [25]. For the convenience of the reader, in Sec. III in the present paper we resume with an example of the formation of such Mie-like resonant mode of the high order when for approaching of particles the resonant modes of each particle are hybridized forming symmetrical (bonding) and antisymmetrical (antibonding) resonant modes.

In addition to disks we consider silicon spheres which are subject to only one-parameter avoided crossing (the distance between spheres). As a result the spheres do not show extremely high-Q factors and respectively giant OB forces but have an advantage of analytical consideration of the OB forces under the illumination of dual counterpropagating Bessel beams. We show that two spheres demonstrate the same features of the OB force which are inherent in the two disks. The optical forces for a single sphere were explicitly derived by Barton *et al.* [26] in a general case that allows one to consider the OB force analytically for the present case of two spheres. The consideration is significantly simplified when the spherical particles are subject to beams such as Gaussian or Bessel if they preserve axial symmetry. Then the binding force depends on the distance between the spheres only [8,14,27–30]. That allows us to derive analytical expressions for the OB force which decreases as $1/L^2$ for exact axial symmetry and $1/L$ otherwise for large distances L between spheres and displays two periods of oscillations as was first revealed by Karásek *et al.* [28] numerically. When the spheres are close to each other the OB force enormously increases if the frequency of Bessel beams follows to the bonding or antibonding resonances. We show also that a magnitude, and what is more interesting, the sign of the OB force, strongly depend on the wave number of the Bessel beams that opens additional options to arrange high-index particles optically.

II. OPTICAL BINDING FORCE OF TWO SPHERES

In order to stabilize the spheres across the beam we use the results by Milne *et al.* [31] that the Bessel beams strongly trap spherical particles at the symmetry axis, i.e., at $r = 0$ (stable zero-force points). That justifies the calculation of the OB as dependent on the distance between the spheres positioned at the symmetry axis. We consider the Bessel beams with TE polarization in the simplest form with zero azimuthal index $m = 0$ [28]

$$\mathbf{E}_{\rm inc}(r, \phi, z) = E_0 \mathbf{e}_\phi \exp(ik_z z) J_1(k_r r), \tag{1}$$

where J_1 is a Bessel function, k_z and k_r are the longitudinal and transverse wave numbers, with the frequency $\omega/c = k = \sqrt{k_r^2 + k_z^2}$ and r, ϕ, and z are the cylindrical coordinates, and $\mathbf{e}_\phi$ is the unit vector of the polarization. In order to consider the OB force we use the approach in which two counterpropagating mutually incoherent Bessel beams were applied [6,8] which are schematically shown in Fig. 1(a).

The electromagnetic (EM) force is defined by the stress tensor $T_{\alpha\beta}$ integrated over the surface elements dS_β outside the particle [32,33]:

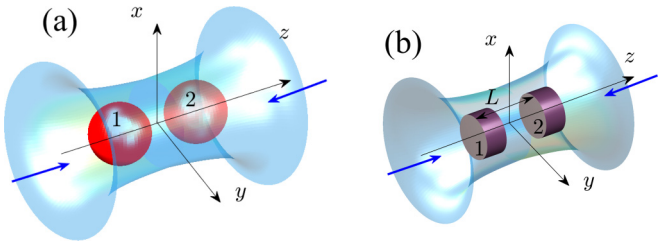

FIG. 1. Two silicon spheres (a) and disks (b) under illumination of two counterpropagating mutually incoherent Bessel beams with zero azimuthal index $m = 0$. L is the distance between centers of particles.

$$F_\alpha = \int T_{\alpha\beta} dS_\beta,$$

$$T_{\alpha\beta} = \frac{1}{4\pi} E_\alpha E_\beta^* - \frac{1}{8\pi}\delta_{\alpha\beta}|\mathbf{E}|^2 + \frac{1}{4\pi} H_\alpha H_\beta^* - \frac{1}{8\pi}\delta_{\alpha\beta}|\mathbf{H}|^2.$$

This problem allows analytical treatment owing to a series of the Bessel beam and scattered fields both over the vectorial spherical harmonics. Such an approach was used to find the optical forces for the case of the isolated sphere [34–38]. In the case of two spheres, multiple scattering theory was used to define the OB forces and calculate them numerically [8,14,27–30]. By using this theory we performed numerical simulations of the complex resonant frequencies and binding force of two coupled spheres with a focus on the dependence of the OB force on the intrinsic parameters such as the distance between spheres and external parameters such as the frequency and wave number of the dual Bessel beams.

The results of the calculations are presented in Figs. 2 and 3 for two values $k_z a = 1/2$ and $k_z a = 1$ of the Bessel beam (1). The parameters of spheres—radius $a = 0.5$ μm, permittivity $\epsilon = 15$, and the intensity of the Bessel beams 1 mW/μm^2—are preserved through all calculations. We show the binding force $F_{\rm OB} = (F_{1z} - F_{2z})/2$ where the indices 1 and 2 denote the spheres where the Bessel beam is incident at the left. Owing to an incoherence of the Bessel beam illuminated from the right we have the same expression for $F_{\rm OB} = -F_{\rm OB}$. As a result we obtain a doubled value for the OB force $F_{\rm OB} = F_{1z} - F_{2z}$. Strong resonant forces above 10 pN by absolute value in Figs. 2 and 3 are saturated by intense red (attractive) or blue (repulsive). As was expected, the OB force shows vivid resonant behavior near the Mie resonances of the individual sphere labeled by orbital index n because of resonant enhancement of scattered fields. However, for variation of the distance between spheres, we see a number of peculiarities. The first one is oscillations when the repulsive OB force is alternated by the attractive one. Respectively, the equilibrium distances shown in Figs. 2 and 3 by solid lines basically follow a law $(k + k_z)L = 2\pi l + \phi_0$, $l = 1, 2, 3, \ldots$ and undergo abrupt changes near the Mie resonances k_n. However there are also long-range oscillations given by the inverse wave number $1/(k - k_z)$. This period will be derived below asymptotically for large L and was first predicted by Karásek *et al.* [28]. Also in Figs. 2 and 3 we show the resonant frequencies of two spheres [even (odd) relative to $z \to -z$ or

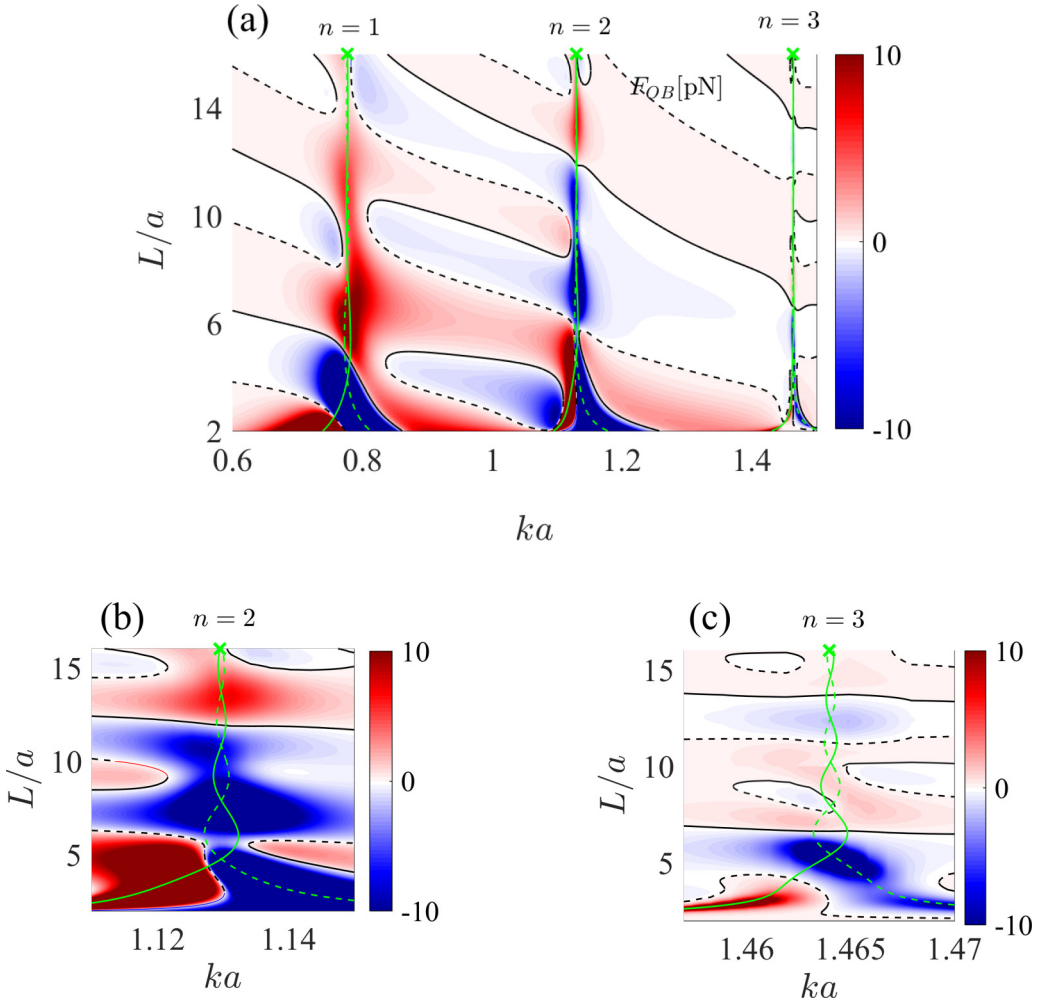

FIG. 2. The binding force vs the frequency and distance between two spheres with radius $a = 0.5$ μm and permittivity $\epsilon = 15$ under illumination of the dual counterpropagating Bessel beams of TE polarization and power 1 mW/μm^2 and $k_z a = 1/2$. (b) and (c) are zoomed versions. The red corresponds to attractive forces and the blue corresponds to repulsive OB force. Black solid (dashed) lines show stable (unstable) configuration of spheres. Light-green solid (dashed) lines show symmetric (antisymmetric) resonant frequencies of two spheres vs the distance between. Crosses mark the Mie TE resonances in an isolated dielectric sphere.

bonding (antibonding)] versus the distance between spheres, which will be analyzed below by the use of multiple scattering theory. The second peculiarity is the decrease of the resonant OB force with the order of the Mie resonance n that will be considered below.

As was said above, the case of two spheres enables analytical treatment of the OB force in the resonant approximation. Owing to the axial symmetry of the total system of two spheres and applied Bessel beam, we can take $m = 0$ with only three components of the EM field, E_ϕ, H_r, and H_θ, for TE polarization in the spherical system. Then outside the spheres the EM fields scattered by the spheres can be presented as a series in the vectorial spherical harmonics as follows [39]:

$$\mathbf{E}(\mathbf{r}) = \sum_n \sum_{j=1,2} b_n^{(j)} \mathbf{M}_{n0}^{(3)}(\mathbf{r} - \mathbf{r_j}), \tag{2}$$

where $\mathbf{r}_j$ are positions of centers of spheres,

$$\mathbf{M}_{n0}^{(3)}(\mathbf{r}) = \mathbf{X}_{n0}(\theta, \phi) h_n(kr), \tag{3}$$

where $\mathbf{X}_{n0}(\theta, \phi)$ are the vector spherical harmonics [40] and $h_n(z)$ are the Hankel functions. Here and below the angular index $m = 0$ in $b_{n0}^{(j)}$ is omitted. For the case of the single sphere the optical forces were explicitly derived by Barton *et al.* [26] in the general case. For the present particular case $m = 0$ the zth component of optical force acting on the first sphere equals

$$F_z^{(1)} = -F_0 \mathrm{Im} \sum_n f_n \left[2 b_{n+1}^{(1)} b_n^{(1)*} + b_{n+1}^{(1)} B_n^{(1)*} + b_n^{(1)*} B_{n+1}^{(1)} \right], \tag{4}$$

where $b_n^{(1)}$ are the coefficients of series (2), $F_0 = \frac{a^4 k^2 E_0^2}{4\pi}$, $f_n = \frac{n(n+1)(n+2)}{\sqrt{(2n+1)(2n+3)}}$, and

$$b_n^{(j)} = S_n(k) B_n^{(j)}, \quad j = 1, 2, \tag{5}$$

where the so-called Lorenz-Mie coefficients are given by

$$S_n(k) = \frac{j_n(\sqrt{\epsilon} ka)[r j_n(kr)]'_{r=a} - j_n(ka)[r j_n(\sqrt{\epsilon} kr)]'_{r=a}}{h_n(ka)[r j_n(\sqrt{\epsilon} kr)]'_{r=a} - j_n(\sqrt{\epsilon} ka)[r h_n(kr)]'_{r=a}}, \tag{6}$$

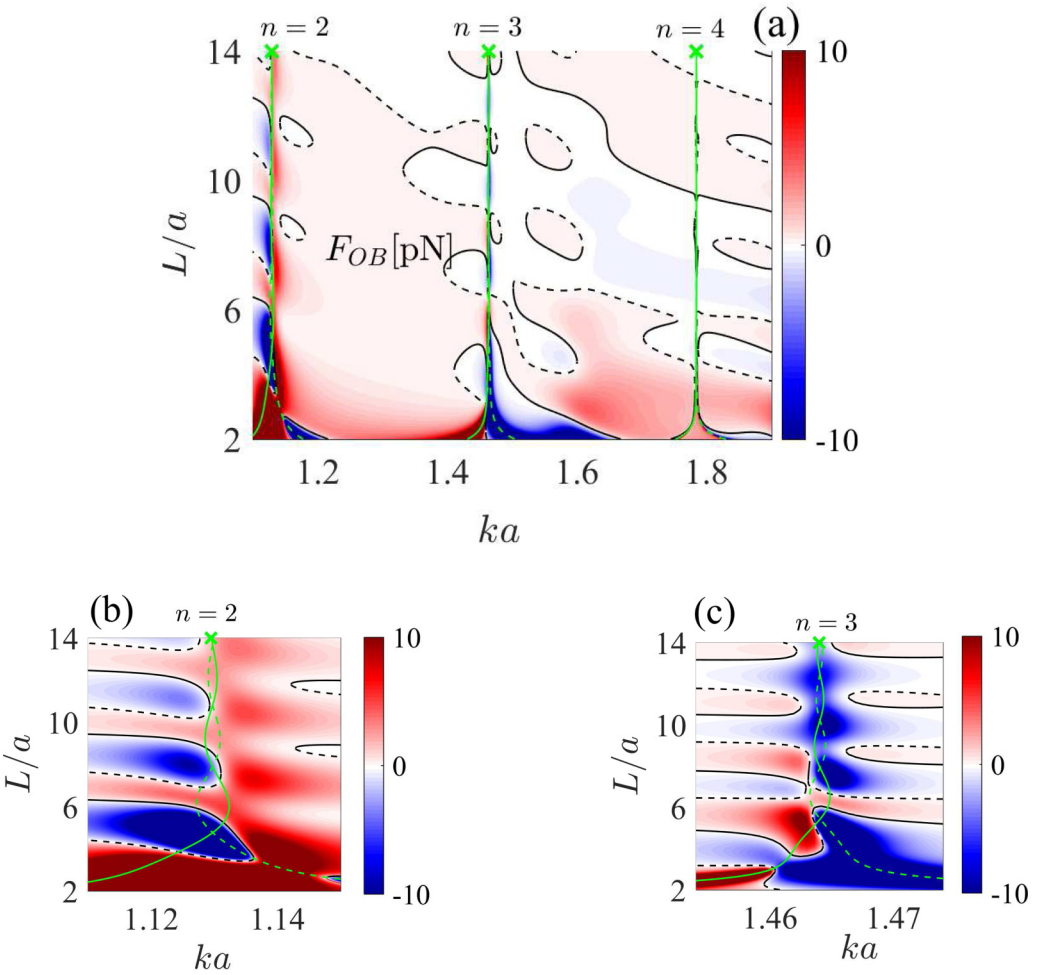

FIG. 3. The same as in Fig. 2 but for $k_z a = 1$.

and $j_n(x)$ are the spherical Bessel functions. The case of two spheres was developed by Thanopulos *et al.* [16]. In contrast to Ref. [16] we reveal that the OB force is basically focused around the Mie resonances for high-index particles. That prompts one to use the resonant approximation which substantially simplifies analysis because of the elimination of the sum over the orbital indices n. Thus, we can truncate the series in Eq. (4) with a preservation of the only resonant term given by the Lorenz-Mie coefficient $S_n(k)$ around the nth Mie resonance. We have for the optical force acting on the jth sphere

$$\frac{F_{zn}^{(j)}}{F_0} \approx \sum_{\sigma=\pm 1} (-1)^{(1+\sigma)/2} f_{n+(\sigma-1)/2} \mathrm{Im}\left[S_n(k)^* B_{n+\sigma}^{(j)} B_n^{(j)*}\right], \quad \sigma = \pm 1. \tag{7}$$

The incident fields radiating the first sphere are superposed of the incident Bessel beam and the field scattered by the second sphere:

$$B_n^{(1)} = B_n^{(\mathrm{inc})} + B_{n,n}^{(21)}(L) b_n^{(2)}, \quad B_{n+\sigma}^{(1)} = B_{n+\sigma}^{(\mathrm{inc})} + B_{n,n+\sigma}^{(21)}(L) b_n^{(2)}. \tag{8}$$

Due to the addition theorem [40,41], we can write the contribution of the second sphere as follows:

$$B_{n,n}^{(21)}(L) = 4\pi \sum_{p=0,2,4,\ldots}^{2n} g_{nnp} i^p \mathcal{G}(n0; n0; p) Y_p^0(1) h_p(kL),$$

$$B_{n,n+1}^{(21)}(L) = 4\pi \sqrt{\frac{n}{(n+2)}} \sum_{p=1,3,5,\ldots}^{2n+\sigma} g_{n,n+1,p} i^p \times \mathcal{G}(n0; n+1, 0; p) Y_p^0(1) h_p(kL), \tag{9}$$

where the argument 1 of Legandre polynomials is related to the direction of the scattered field. Substituting the specific expressions for the spherical Bessel functions into Eq. (9) with account of coefficients g and $\mathcal{G}$ tabulated in Ref. [40], we find for $kL \gg 1$

$$B_{n,n}^{(21)}(L) \approx -c_{n,n} \frac{e^{ikL}}{(kL)^2}, \quad B_{n,n+\sigma}^{(21)}(L) \approx -i c_{n,n+\sigma} \frac{e^{ikL}}{(kL)^2}, \tag{10}$$

where $c_{1,1} = 3$, $c_{2,2} = 15, c_{1,2} = 6.708$, $c_{2,3} = 25.1, \ldots$ are real coefficients.

For the large kL we can rewrite Eq. (8) as follows:

$$B_n^{(1)} \approx B_n^{(\mathrm{inc})}\left[1 + B_{n,n}^{(21)}(L)S_n(k)e^{ik_zL}\right],$$
$$B_{n+\sigma}^{(1)} \approx B_{n+\sigma}^{(\mathrm{inc})} + B_{n,n+\sigma}^{(21)}(L)S_n(k)B_n^{(\mathrm{inc})}e^{ik_zL}, \quad (11)$$

where we took into account that the Bessel beam (1) accumulates the phase factor e^{ik_zL} when it reaches the second sphere. Substituting here asymptotes (10) and using an inequality $|B_n^{(\mathrm{inc})}| \gg |B_{n,n}^{(21)}(L)b_n^{(2)}|$ we can approximate

$$B_n^{(1)} \approx B_n^{(\mathrm{inc})}\left[1 - \frac{S_n(k)}{(kL)^2}c_{n,n}e^{i(k_z+k)L}\right],$$
$$B_{n+\sigma}^{(1)} \approx B_{n+\sigma}^{(\mathrm{inc})} - \frac{iS_n(k)}{(kL)^2}c_{n,n+\sigma}B_n^{(\mathrm{inc})}e^{i(k_z+k)L}. \quad (12)$$

As a result we obtain the following expression for the optical force (7) onto the first sphere:

$$F_{zn}^{(1)} \approx F_0\sum_{\sigma=\pm1}(-1)^{(1+\sigma)/2}f_{n+(\sigma-1)/2}\Big[\mathrm{Im}\left(S_n^*B_n^{(\mathrm{inc})*}B_{n+\sigma}^{(\mathrm{inc})}\right)$$
$$-\frac{c_{n,n}}{(kL)^2}\left|S_n^2B_n^{(\mathrm{inc})}B_{n+\sigma}^{(\mathrm{inc})}\right|\sin[(k+k_z)L+\phi_{n+\sigma}]$$
$$-\frac{c_{n,n+\sigma}}{(kL)^2}\left|B_n^{(\mathrm{inc})}S_n\right|^2\cos(k+k_z)L\Big], \quad (13)$$

where $\phi_{n+\sigma} = \arg(B_n^{(i)}B_{n+\sigma}^{(inc)*}S_n(k)^2)$. Similarly, we have for the second sphere

$$B_n^{(2)} = B_n^{(\mathrm{inc})}e^{ik_zL} + B_{n,n}^{(12)}(L)b_n^{(1)},$$
$$B_{n+\sigma}^{(2)} = B_{n+\sigma}^{(\mathrm{inc})}e^{ik_zL} - B_{n,n+\sigma}^{(12)}(L)b_n^{(1)}. \quad (14)$$

By use of identities

$$B_{n,n}^{(21)} = B_{n,n}^{(12)}, \quad B_{n,n+\sigma}^{(21)} = -B_{n,n+\sigma}^{(12)} \quad (15)$$

and Eq. (10) we can rewrite Eq. (14) as follows:

$$B_n^{(2)} = B_n^{(\mathrm{inc})}\left[e^{ik_zL} - \frac{c_{n,n}}{(kL)^2}S_ne^{ikL}\right],$$
$$B_{n+\sigma}^{(2)} = B_{n+\sigma}^{(\mathrm{inc})}e^{ik_zL} + \frac{ic_{n,n+\sigma}}{(kL)^2}S_nB_n^{(\mathrm{inc})}e^{ikL}. \quad (16)$$

As a result we have for the force acting on the second sphere

$$F_{zn}^{(2)} \approx F_0\sum_{\sigma=\pm1}(-1)^{(1+\sigma)/2}f_{n+(\sigma-1)/2}\Big\{\mathrm{Im}\left(S_n^*B_n^{(\mathrm{inc})*}B_{n+\sigma}^{(\mathrm{inc})}\right)$$
$$+\frac{c_{n,n}}{(kL)^2}\left|S_n^2B_n^{(\mathrm{inc})}B_{n+\sigma}^{(\mathrm{inc})}\right|\sin[(k-k_z)L-\phi_{n+\sigma}]$$
$$+\frac{c_{n,n+\sigma}}{(kL)^2}\left|B_n^{(\mathrm{inc})}S_n\right|^2\cos(k-k_z)L\Big\}, \quad (17)$$

i.e.,

$$F_{zn}^{(2)}(k_z) = -F_{zn}^{(1)}(-k_z). \quad (18)$$

Therefore, the asymptotes at $kL \gg 1$ for OB force owing to the dual Bessel beams propagating along the z axis equal

$$F_{\mathrm{OB}}(L) = F_{zn}^{(1)}(k_z) - F_{zn}^{(2)}(k_z) \approx F_0\sum_{\sigma=\pm1}(-1)^{(1+\sigma)/2}f_{n+(\sigma-1)/2}$$
$$\times\Big\{\frac{c_{n,n}}{(kL)^2}\Big[\left|S_n^2B_n^{(\mathrm{inc})}B_{n+\sigma}^{(\mathrm{inc})}\right|\sin[(k+k_z)L+\phi_{n+\sigma}]$$
$$+\sin[(k-k_z)L+\phi_{n+\sigma}]\Big]$$
$$+\frac{c_{n,n+\sigma}}{(kL)^2}\left|B_n^{(\mathrm{inc})}S_n\right|^2[\cos(k+k_z)L+\cos(k-k_z)L]\Big\}. \quad (19)$$

This expression shows two properties of the OB for long distances between spheres: the long-distance and short-range modulation of the binding force $\frac{2\pi}{k-k_z}$ and $\frac{2\pi}{k+k_z}$ that was reported by Karásek *et al.* [28] numerically by use of a coupled dipole method. It is worthy to note that the oscillatory behavior of the OB was observed already by Burns *et al.* [5] that was used for separation of 1.43 μm polystyrene particles in water. An asymptotical decline $1/L^2$ of the OB force can be also understood if we consider the scattered field from the second sphere positioned at the z axis at the distance L is given by the vector spherical function [40]

$$\mathbf{M}_{n0}(\mathbf{r}-\mathbf{e}_zL) = -\mathbf{e}_\phi h_n(kL)\frac{dP_n^0(\cos\theta)}{d\theta}. \quad (20)$$

For integration over the first sphere positioned at $z=0$ the contribution of the second sphere is proportional to $\sin\theta = a/L$. As a result, together with the asymptotic of the Bessel function $h_n(kL) \sim \frac{e^{ikL}}{kL}$ we obtain the total asymptotic $1/L^2$. We notice that this asymptotic agrees with the result derived by Thirunamachandran using a different method of quantum electrodynamics when the polarization of the beam is directed along the x axis [Eq. (16) of Ref. [2]]. However, this asymptotic is justified only for exact coaxial illumination of spheres by the Bessel beams which do not carry angular momentum. As soon as the direction of the Bessel beam is tilted to the z axis or carries the angular momentum, we obtain typical asymptotic $1/L$ that again coincides with the results by Thirunamachandran [Eq. (19) of Ref. [2]].

The behavior of OB at the close vicinity of spheres $L \to 2a$ is more dramatic as Fig. 4 demonstrates. In order to analytically evaluate this behavior we employ the multiple scattering theory which reduces the Maxwell equations into the linear algebraic equations for the amplitudes b_n in expansions of EM fields over vectorial spherical harmonics (2) given by the index n and $m=0$ which can be written as matrix equation

$$\widehat{L}(k)\vec{\psi} = \vec{\psi}_{\mathrm{inc}}, \quad (21)$$

where the non-Hermitian, nonsymmetric matrix $\widehat{L}(k)$ is determined by a specific structure of dielectric particles. The incident state $\vec{\psi}_{\mathrm{inc}}$ is the column of amplitudes $B_n^{(\mathrm{inc})}$ in this representation. The resonances are given by the solutions of the homogeneous equation

$$\widehat{L}(k)\vec{\psi} = 0 \quad (22)$$

for complex eigenvalues k whose real parts are shown by solid and dashed lines in Figs. 2(b) and 2(c). For the present problem it is important to note that the matrix $\widehat{L}(k)$ can be defined in the basis of left and right eigenvectors

$$\vec{y}_\lambda\widehat{L}(k) = \lambda\vec{y}_\lambda, \quad \widehat{L}(k)\vec{x}_\lambda = \lambda\vec{x}_\lambda, \quad (23)$$

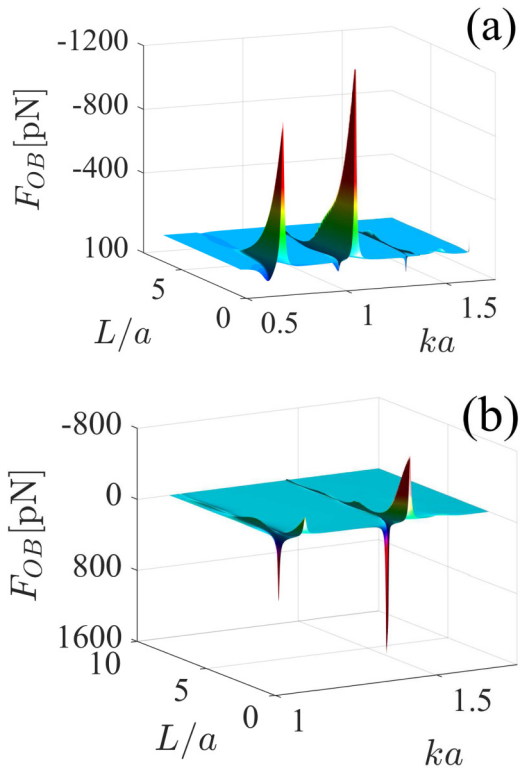

FIG. 4. The binding force between two spheres vs the wavelength and distance for (a) $k_z a = 1/2$ and (b) $k_z a = 1$.

where $\vec{y}_\lambda \vec{x}_{\lambda'} = \delta_{\lambda,\lambda'}$. By using the condition of completeness

$$\sum_\lambda \vec{x}_\lambda \vec{y}_\lambda = 1, \tag{24}$$

we write the following equalities:

$$\widehat{L}(k) = \sum_\lambda \lambda \vec{x}_\lambda \vec{y}_\lambda, \quad \widehat{L}^{-1}(k) = \sum_\lambda \frac{\vec{x}_\lambda \vec{y}_\lambda}{\lambda}, \tag{25}$$

as well as for the solution of Eq. (21),

$$\vec{\psi} = \sum_\lambda \frac{W_\lambda}{\lambda} \vec{x}_\lambda, \tag{26}$$

where

$$W_\lambda = \vec{y}_\lambda \vec{\psi}_{\rm inc} \tag{27}$$

are the coupling coefficients of the incident wave with the eigenmodes of the open system. For the case of high refractive index of dielectric sphere the index λ can be related to those resonant terms which have the smallest λ_n in the vicinity of the resonant frequency $k \approx {\rm Re}(k_n)$. That allows one to write, in the vicinity of the nth Mie resonant frequency ${\rm Re}(k_n)$, the eigenvalue as

$$\lambda_n = q_n(k - k_n). \tag{28}$$

For the case of identical high-index particles resonant modes can be presented as symmetric (bonding) and antisymmetric (antibonding) modes [42]

$$\mathbf{E}_n \approx \frac{E_0 W_{n,s}}{(k - k_{n,s})} \mathbf{E}_{n,s} + \frac{E_0 W_{n,a}}{(k - k_{n,a})} \mathbf{E}_{n,a}, \tag{29}$$

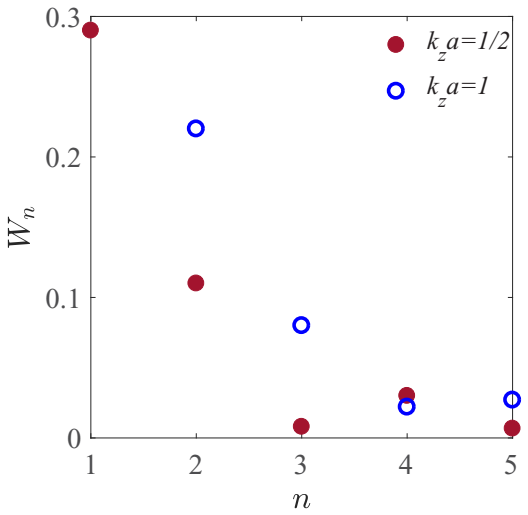

FIG. 5. The coupling coefficient $W_n(k, k_z)$ vs the order of Mie resonance n.

where the factors $1/q_n$ are absorbed by the coupling constants $W_{n,s,a}$,

$$\mathbf{E}_{n,s,a}(\mathbf{r}) \approx \frac{1}{\sqrt{2}} \left[\mathbf{M}_{n0}\left(\mathbf{r} - \frac{L}{2}\mathbf{e}_z\right) \pm \mathbf{M}_{n0}\left(\mathbf{r} + \frac{L}{2}\mathbf{e}_z\right) \right]. \tag{30}$$

E_0 is the amplitude of the Bessel beam. The coupling constant of incident Bessel beam (1) with the symmetric or antisymmetric resonant modes (30) can, according to the definition (27), be presented as (see also [43])

$$W_{n,s,a} \approx W_n(k, k_z) \begin{cases} \cos k_z L/2 \\ i \sin k_z L/2 \end{cases}, \tag{31}$$

where $W_n(k, k_z)$ is the coupling constant of the Bessel beam with the nth Mie resonant mode. One can perform analytical calculations of the constant by the use of a great deal of algebra presented in Refs. [37,38,44,45]. However, it is simpler to find the coupling constants numerically because their values are independent on the distance. The results are presented in Fig. 5 for $k_z a = 0.5, 1$ and show that the OB force decreases with n. Thus, although the Q factor rapidly grows with the order of the Mie resonances [46], the coupling of the corresponding resonant mode with the Bessel beams decays even more to result in a weakening of the OB forces with n.

The resonant frequencies in the two-level approximation can be written as follows [42]:

$$k_{n,s,a} = {\rm Re}(k_{n,s,a}) - i\gamma_{n,s,a} \approx k_n \pm \frac{v_n}{L^2} e^{i(k_n L - \theta_n)}. \tag{32}$$

Figure 6 shows that the resonant frequencies (32) well describe numerically calculated dipole resonances $n = 1$ with fitting parameters $v_1 = 0.15$ and $\theta_1 = 1.25$. As seen from Figs. 2 and 3, at close distances between spheres the bonding and antibonding resonances are well separated which allows us to consider them independently. In what follows we consider in detail the antibonding dipole resonance $n = 1$ for which the OB noticeably exceeds the case of the bonding resonance as Fig. 4(a) shows. The reason is related to the denominators in Eq. (29) which equal the imaginary

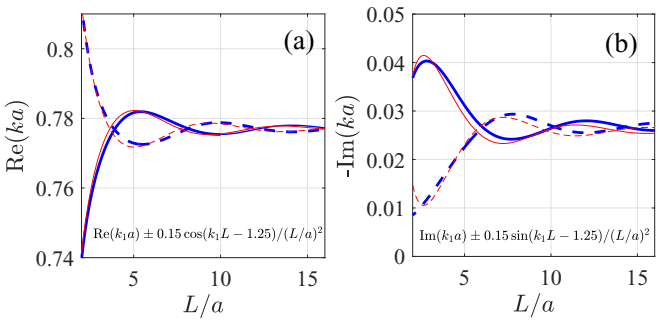

FIG. 6. The dipole $n = 1$ resonant frequencies of two coupled spheres, real (a) and imaginary (b), vs the distance calculated from Eq. (22) (thick blue) and compared to two-level approximation (32) (thin red) and presented with fitting parameters in figures. Solid (dashed) lines show the frequencies of bonding (antibonding) resonances.

parts of the resonances $\mathrm{Im}(k_{n,s,a})$ at $k = \mathrm{Re}(k_{n,s,a})$. In other words, the near fields are proportional to the quality factors $Q_{n,s,a} = -\mathrm{Re}(k_{n,s,a})/2\mathrm{Im}(k_{n,s,a})$. For the dipole case resonances with $n = 1$ the $Q_{1,s} \to 10$ while $Q_{1,a} \to 56$ at $L \to 2a$. The response of the scattered field around the antibonding resonance becomes strong compared to the incident Bessel beam. Therefore the incident field can be neglected. Figure 7(a) demonstrates that the scattered field indeed slightly differs from the antisymmetric mode $\vec{E}_{n,a}$ given by Eq. (30). That directly correlates with the behavior of the resonant width vs L shown in Fig. 6(b). One can see that $\mathrm{Im}(k_{1,a})$ has a minimum at $L \approx 2a$, while Fig. 7(b) shows that the Bessel beam contributes significantly into the scattered field when $k \approx k_{1,s}$ and therefore cannot be disregarded. That is a consequence of the resonant width of the antibonding dipole resonant mode 1, s. One can see from Fig. 6(b) that the resonant width of the bonding dipole resonant mode 1, s reaches maximum for $L \to 2a$.

A comparison of Eq. (29) with Eq. (5) gives us

$$b_n^{(j)} = (-1)^{j-1} E_0 d_n, \quad j = 1, 2, \tag{33}$$

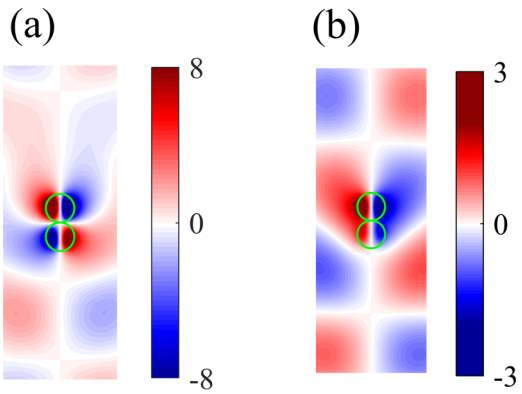

FIG. 7. Numerically computed scattered field (the component E_ϕ) at the closest distance $L = 2a$ for frequencies around the dipole Mie resonance k_1: (a) $k = \mathrm{Re}(k_{1,a})$ (antibonding resonant mode), (b) $k = \mathrm{Re}(k_{1,s})$ (bonding resonant mode). The Bessel beam with $k_z a = 0.5$ illuminates spheres from the bottom.

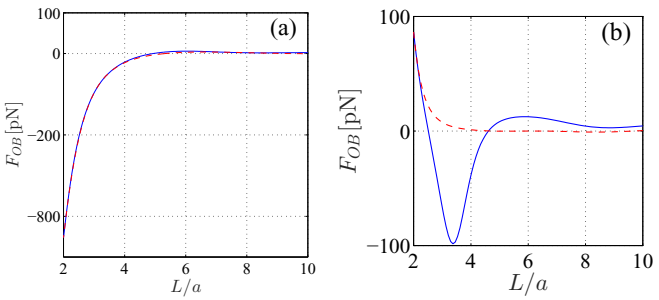

FIG. 8. The OB vs the distance between spheres at the vicinity of the dipole antibonding (a) resonance $k = \mathrm{Re}[k_{1,a}(L)]$ and (b) bonding resonance $k = \mathrm{Re}[k_{1,s}(L)]$. The solid line shows numerics and the dashed line shows approximated formulas. Wave number of the Bessel beam $k_z a = 1/2$.

where $d_n = \frac{W_{n,a}}{\sqrt{2} q \gamma_{n,a}} \sin(k_z L/2)$. Owing to Eqs. (5) and (8) we have

$$B_n^{(1)} \approx d_n \Big(\frac{1}{S_n(k_n)} - B_{n,n}^{(21)}(L) \Big),$$
$$B_{n+1}^{(1)} \approx B_{n,n+1}^{(21)}(L) b_n^{(2)} = -d_n B_{n,n+1}^{(21)}(L). \tag{34}$$

According to Eq. (4) we obtain for the force acting onto the first sphere around the antibonding dipole resonance $k \approx \mathrm{Re}(k_{1,a})$

$$\frac{F_{z1}^{(1)}}{F_0} \approx -\mathrm{Im}\big(S_1^* B_1^{(1)*} B_2^{(1)}\big)$$
$$\approx -|d_1|^2 \big\{ \mathrm{Im}\big[1 - S_1 B_{1,2}^{(21)*}(L)\big]\big[1 + B_{1,1}^{(21)*}(L)\big] \big\}, \tag{35}$$

where

$$B_{1,1}^{(21)}(L) = h_0(kL) + h_2(kL),$$
$$B_{1,2}^{(21)}(L) = -1.3416[h_1(kL) + h_3(kL)]$$

owing to Eq. (9). Taking into account relations (15) we obtain the OB at $L \geqslant 2a$

$$\frac{F_{\mathrm{OB}}}{F_0} = 2\frac{F_{z1}^{(1)}}{F_0} = \frac{1.3416 f_1 |W_1|^2 \sin^2(k_z L/2)}{\gamma_{1,a}^2(L)} \mathrm{Im}\{[1 - S_1^*(k_{1,a})]$$
$$\times [h_0^*(kL) + h_2^*(kL)][h_1(kL) + h_3(kL)]\}. \tag{36}$$

Figure 8(a) shows the asymptotic formula (36) perfectly describes the numerically computed OB force for the dipole antibonding resonance. A similar asymptotic formula can be written for the bonding resonance by simple substitution $a \to s$. However, Fig. 8(b) shows a strong discrepancy between the numerics and asymptotic formula. The discrepancy is related to that as seen from Fig. 6(b); the bonding resonant width reaches maximum at $L \to 2a$. As a result, enhancement of the scattered EM field at the bonding resonance roughly four times yields to the case of antibonding resonance. Therefore for calculation of the optical forces we cannot neglect the incident fields as distinct from the dipole antibonding resonance.

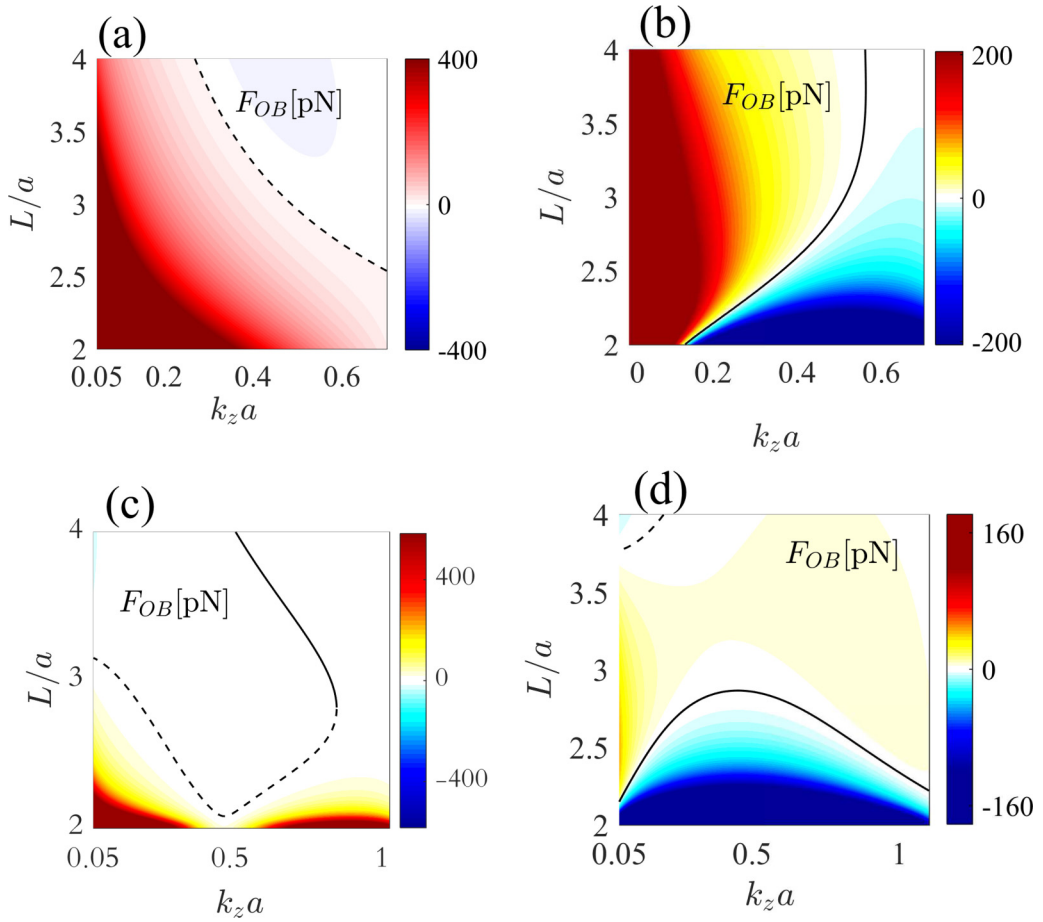

FIG. 9. The OB vs distance between spheres and the longitudinal wave number of the Bessel beam at the vicinity of the TE Mie resonances. (a) $ka = 0.735$ around the bonding dipole resonance $n = 1$, (b) $ka = 0.82$ around the antibonding dipole resonance $n = 1$, (c) $ka = 1.0947$ around the bonding quadrupole resonance $n = 2$, and (d) $ka = 1.1783$ around the antibonding quadrupole resonance at $L = 2a$. The solid line shows the equilibrium positions of spheres.

Next, with growth of the order of the Mie TE resonances n in the dielectric sphere the resonant width exponentially decreases [46,47]. Therefore one could expect the fast growth of the OB force. However, by the same reason of reduction of radiation losses with n decrease of the coupling of the Mie resonant modes with the Bessel beam occurs which Fig. 5 demonstrates.

Moreover two parameters, the frequency and by wave vector k_z along the propagation axis z, define the Bessel beam (1). Figures 2 and 3 show that indeed these parameters noticeably affect the equilibrium distances between the spheres. Equation (36) predicts simple dependence of the OB on the longitudinal wave number k_z of the Bessel beam in the form of $\sin^2 k_z L/2$ but rather complicated dependence on the distance L through the Hankel functions for the antibonding dipole resonance. This conclusion is illustrated in Fig. 9 which shows strong dependence of the OB force on k_z and L for frequencies tuned to the dipole and quadrupole antibonding frequencies $\mathrm{Re}(k_{1,a})$ and $\mathrm{Re}(k_{2,a})$, respectively. One can see that these results provide a potentially useful way to manipulate the distance between particles by variation of the longitudinal wave number of the Bessel beams.

III. OPTICAL BINDING FORCE BETWEEN TWO COAXIAL DISKS

Distinct to the case of two spheres, two disks have two parameters to vary: the aspect ratio and distance between disks. Even in an isolated dielectric disk the high-Q resonances can be achieved by avoided crossing of the TE resonances of the same symmetry relative to inversion of the disk's axis under variation of the aspect ratio around $a/h = 0.71$ as was reported by Rybin *et al.* [48] and illustrated in Figs. 10(a) and 10(b). While the resonances of the opposite symmetry in an isolated disk plotted by solid and dashed lines cannot be coupled in a single disk. An example of this crossing is highlighted by the circle in Fig. 10(a). However, the presence of the second disk lifts this symmetry restriction giving rise to a new series of avoided crossings of resonances shown in Fig. 10(c) [25]. In view of the OB force the most important is the antibonding resonance which achieves a high-Q factor of around 18 000 as shown in Fig. 10(d). The reason for such an extreme value is related to the fact that the antibonding resonant mode is close to the Mie resonant mode with an extremely large orbital index ($n = 6$) of an effective sphere with the volume equal to $\pi(h + L)a^2$ shown in the right bottom inset of Fig. 10(c) [25]. That refers also to the bonding reso-

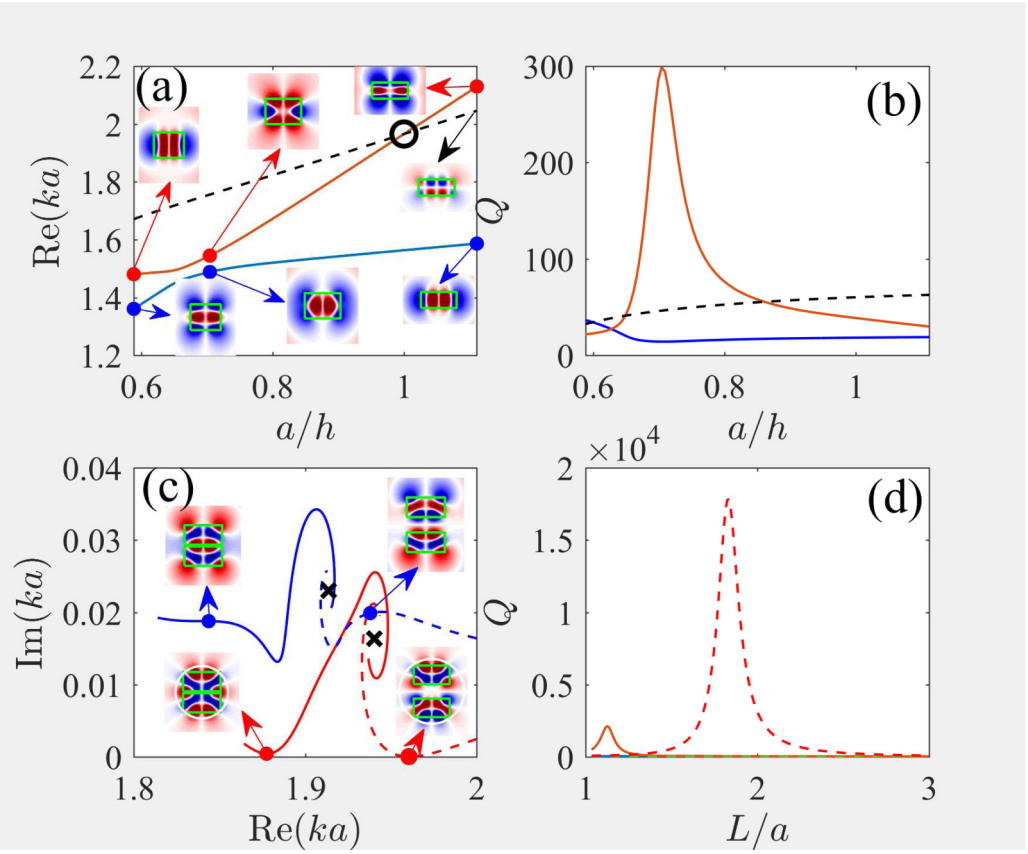

FIG. 10. (a) Avoided crossing of two TE resonances whose modes are symmetric relative to $z \to -z$ for traversing over distance and (b) their Q factors versus the aspect ratio a/h in an isolated silicon disk. (c) Behavior of hybridized resonances and (d) the Q factor vs distance between centers of disks for $a/h = 1.003$. Insets show the profiles of tangential components of electric field E_ϕ.

nant mode which is close to the Mie resonant mode with $n = 5$ shown in the left bottom inset in Fig. 10(c). Respectively, we expect around the aspect ratio $a/h = 1$ extremal enhancement of OB, especially for the antibonding resonant mode similar to Refs. [17–19]. These effective spheres are shown by white lines in the bottom insets.

First, we consider a stability of single disk at $r = 0$. Numerical calculations of forces by the centered Bessel beam and slightly shifted beam relative to axis $r = 0$ have shown that the position of the disk is stable at the symmetry axis at the vicinity of resonant frequencies. That considerably simplifies the further calculation of the OB between two disks. The results of calculations of the OB are presented in Figs. 11 and 12. Figure 12 demonstrates that indeed near the parameters of extremely large peaks of the Q factor we observe, respectively, giant OB of order 1 nN. For the reader's convenience we reproduce Fig. 11 as the surface in Fig. 12(a) where one can see that giant OB is achieved around 30 nN at $ka = 1.97$, $L =$

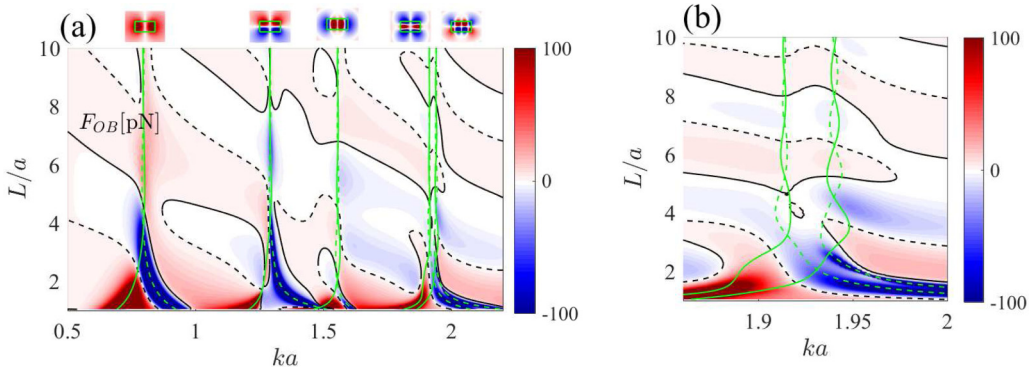

FIG. 11. The binding force between two disks vs the frequency and distance between centers of disks for the Bessel beam with TE polarization and $k_z a = 1/2$ where the disk with $\epsilon = 15$ has the radius $a = 0.5$ μm. (b) Zoomed versions. Black solid (dashed) lines show stable (unstable) configuration of disks. Light-green solid (dashed) lines show bonding (symmetric) and antibonding (antisymmetric) resonant frequencies of two disks vs the distance between.

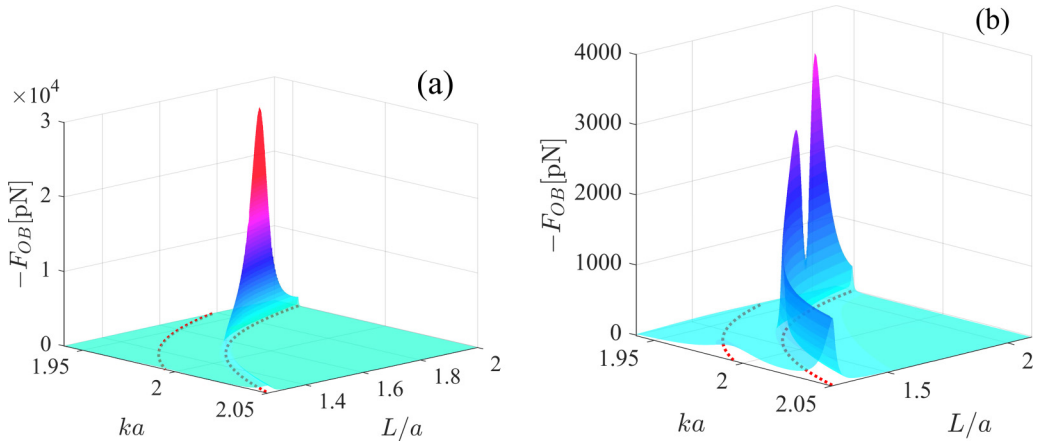

FIG. 12. The OB vs distance between centers of disks at the vicinity of the antibonding resonance marked in Fig. 10(c) by closed circle $ka = 1.95$: (a) $k_z a = 0.5$ and (b) $k_z a = 1$. Solid line underneath shows resonant frequency vs distance L highlighted in Fig. 11.

$1.85a$, $h = 1.03a$, and $k_z a = 0.5$. Figure 12(b) shows that this giant peak is split for $k_z a = 1$. It is remarkable that the equilibrium distances between disks are traversed close to the antibonding resonance shown by a dotted line. That situation was first reported for two dielectric slabs which can move in a waveguide that is equivalent to a Fabry-Perot resonator with high-Q resonances [49]. Figure 13 demonstrates that these giant peaks are easily manipulated by small changes of parameters of the Bessel beam: $k_z a$ and frequency.

IV. SUMMARY AND CONCLUSIONS

In the present paper we consider OB of particles of micron size by illumination of dual counterpropagating Bessel beams. The case of two spheres owing to formulas derived by Barton *et al.* [26] for electromagnetic force acting on the isolated sphere gives an opportunity to derive analytical expressions for the OB force in the resonant approximation. At large distances the OB force decays as inverse squared distance and has two periods of oscillations [Eq. (19)]. For near distances the OB force can be considerably enhanced up to an order of 1 nN. One of the important and unexpected results of the OB forces of spheres is their decrease with growth of the order of the Mie resonances. That is a result of the competition of two types of couplings. The first coupling of the Mie resonant modes of the sphere with the radiation continua given by the vectorial spherical functions fast falls with growth of the order of resonance giving rise to WGMs with extremal Q factors [46,47]. However, the couplings of the Mie resonant modes with the incident Bessel beams can decay even faster with the growth of the order of the Mie resonant mode. Indeed, our calculations presented in Fig. 4 show that the OB force is large only for the dipole and quadrupole Mie resonances.

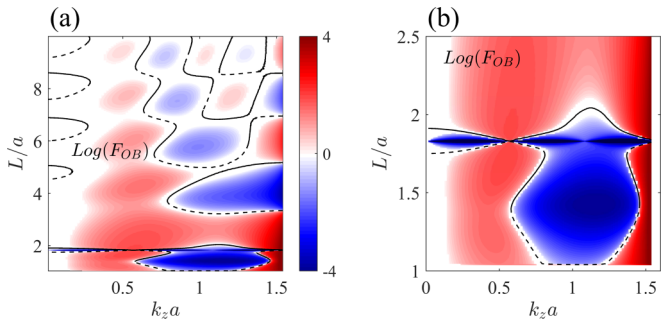

FIG. 13. (a) The OB vs distance between disks and longitudinal wave vector of the Bessel beam $k_z a$ at the vicinity of the antibonding resonance marked in Fig. 10(c) by closed circle $ka = 1.95$. (b) Zoomed version of (a).

The case of coaxial disks brings a new aspect to the OB force related to the extremely high-Q factor due to the two-parametric avoided crossing of orthogonal resonances over aspect ratio and distance between the disks [25]. For the case of two coaxial silicon disks with micron diameter illuminated by dual coaxial Bessel beams we demonstrate giant OB force in few tens of nanonewtons in the vicinity of antibonding resonances. The terminology "giant" means that the forces of order of 1 nN exceed the van der Waals forces, at least, by three orders and gravitational forces by five orders [17]. The corresponding antibonding resonant mode of two disks turns out to be close to the Mie resonant mode with high orbital index $n = 6$ of an effective sphere of the volume $\pi a^2(h + L)$ [25] with an extremely high-Q factor. That allows one to achieve giant OB force around several tens of nanonewtons.

There are three important aspects of the OB force of two high-index dielectric particles. The first is a giant value of the force around 1 nN for two spheres and a few tens of nanonewtons for two coaxial disks illuminated by dual Bessel beams with power 1 mW/μm^2. The second aspect is that the giant OB forces are caused by resonant excitation of *subwavelenth* resonant modes of particles. A potentially easy way for cardinal manipulation of the OB force by a cross section of the Bessel beam constitutes the third aspect of the presented results. The reader can easily find dimensional units instead of dimensionless value $x = ka$ via $a = 0.5$ μm. In terms of the light wavelength we obtain that the characteristic resonant features lie in the range of micron wavelengths.

ACKNOWLEDGMENTS

This work was supported by Russian Foundation for Basic Research Project No. 19-02-00055. A.S. thanks D. Maksimov and E. Sherman for helpful discussions.

[1] A. Ashkin, J. M. Dziedzic, J. E. Bjorkholm, and S. Chu, Opt. Lett. **11**, 288 (1986).

[2] T. Thirunamachandran, Mol. Phys. **40**, 393 (1980).

[3] D. S. Bradshaw and D. L. Andrews, Phys. Rev. A **72**, 033816 (2005).

[4] K. A. Forbes, D. S. Bradshaw, and D. L. Andrews, Nanophotonics **9**, 1 (2019).

[5] M. M. Burns, J.-M. Fournier, and J. A. Golovchenko, Phys. Rev. Lett. **63**, 1233 (1989).

[6] S. A. Tatarkova, A. E. Carruthers, and K. Dholakia, Phys. Rev. Lett. **89**, 283901 (2002).

[7] R. Gómez-Medina and J. J. Sáenz, Phys. Rev. Lett. **93**, 243602 (2004).

[8] N. K. Metzger, K. Dholakia, and E. M. Wright, Phys. Rev. Lett. **96**, 068102 (2006).

[9] N. K. Metzger, E. M. Wright, and K. Dholakia, New J. Phys. **8**, 139 (2006).

[10] K. Dholakia and P. Zemánek, Rev. Mod. Phys. **82**, 1767 (2010).

[11] R. Bowman and M. Padgett, Rep. Prog. Phys. **76**, 026401 (2013).

[12] I. Thanopulos, D. Luckhaus, and R. Signorell, Phys. Rev. A **95**, 063813 (2017).

[13] P. C. Chaumet and M. Nieto-Vesperinas, Phys. Rev. B **64**, 035422 (2001).

[14] J. Ng, Z. Lin, C. Chan, and P. Sheng, Phys. Rev. B **72**, 085130 (2005).

[15] T. Čižmár, V. Kollárová, Z. Bouchal, and P. Zemánek, New J. Phys. **8**, 43 (2006).

[16] I. Thanopulos, D. Luckhaus, T. Preston, and R. Signorell, J. Appl. Phys. **115**, 154304 (2014).

[17] M. I. Antonoyiannakis and J. B. Pendry, Europhys. Lett. **40**, 613 (1997).

[18] V. Liu, M. Povinelli, and S. Fan, Opt. Express **17** (2009).

[19] J. Zhang, K. MacDonald, and N. Zheludev, Opt. Lett. **39**, 4883 (2014).

[20] A. Taghizadeh and I.-S. Chung, Appl. Phys. Lett. **111**, 031114 (2017).

[21] Z. F. Sadrieva, M. A. Belyakov, M. A. Balezin, P. V. Kapitanova, E. A. Nenasheva, A. F. Sadreev, and A. A. Bogdanov, Phys. Rev. A **99**, 053804 (2019).

[22] E. N. Bulgakov and A. F. Sadreev, Phys. Rev. A **99**, 033851 (2019).

[23] M. L. Povinelli, S. Johnson, M. Loncar, M. Ibanescu, E. Smythe, F. Capasso, and J. D. Joannopoulos, Optics Express **13**, 8286 (2005).

[24] M. Benyoucef, J.-B. Shim, J. Wiersig, and O. G. Schmidt, Opt. Lett. **36**, 1317 (2011).

[25] E. N. Bulgakov, K. N. Pichugin, and A. F. Sadreev, arXiv:2005.05554.

[26] J. P. Barton, D. R. Alexander, and S. A. Schaub, J. Appl. Phys. **66**, 4594 (1989).

[27] V. Karásek and P. Zemánek, J. Opt. A: Pure Appl. Opt. **9**, S215 (2007).

[28] V. Karásek, O. Brzobohatý, and P. Zemánek, J. Opt. A: Pure Appl. Opt. **11**, 034009 (2009).

[29] Y. Zhu, Z. Wu, Z. Li, and Q. Shang, Proc. Eng. **102**, 329 (2015).

[30] F. Deng, H. Liu, M. Panmai, and S. Lan, Opt. Express **26**, 20051 (2018).

[31] G. Milne, K. Dholakia, D. McGloin, K. Volke-Sepulveda, and P. Zemánek, Opt. Express **15**, 13972 (2007).

[32] L. D. Landau and E. M. Lifshitz, *Electrodynamics of Continuous Media* (Pergamon, New York, 1960).

[33] M. I. Antonoyiannakis and J. B. Pendry, Phys. Rev. B **60**, 2363 (1999).

[34] J. Chen, J. Ng, S. Liu, and Z. Lin, Phys. Rev. E **80**, 026607 (2009).

[35] N. Wang, J. Chen, S. Liu, and Z. Lin, Phys. Rev. A **87**, 063812 (2013).

[36] S. Song, N. Wang, W. Lu, and Z. Lin, J. Opt. Soc. Am. A **31**, 2192 (2014).

[37] A. D. Kiselev and D. O. Plutenko, Phys. Rev. A **94**, 013804 (2016).

[38] A. Neves and C. Cesar, J. Opt. Soc. Am. B **36**, 1525 (2019).

[39] J. Stratton, *Electromagnetic Theory* (McGraw-Hill, New York, 1941).

[40] C. Linton, V. Zalipaev, and I. Thompson, Wave Motion **50**, 29 (2013).

[41] D. Mackowski, Proc. R. Soc. London, Ser. A **433**, 599 (1991).

[42] K. N. Pichugin and A. F. Sadreev, J. Appl. Phys. **126**, 093105 (2019).

[43] Q. Song, M. Zhao, L. Liu, J. Chai, G. He, H. Xiang, D. Han, and J. Zi, Phys. Rev. A **100**, 023810 (2019).

[44] A. S. van de Nes and P. Torok, Opt. Express **15**, 13360 (2007).

[45] Y. Jiang, Y. Shao, X. Qu, J. Ou, and H. Hua, J. Opt. **14**, 125709 (2012).

[46] C. C. Lam, P. T. Leung, and K. Young, J. Opt. Soc. Am. B **9**, 1585 (1992).

[47] M. L. Gorodetsky, A. A. Savchenkov, and V. S. Ilchenko, Opt. Lett. **21**, 453 (1996).

[48] M. V. Rybin, K. L. Koshelev, Z. F. Sadrieva, K. B. Samusev, A. A. Bogdanov, M. F. Limonov, and Y. S. Kivshar, Phys. Rev. Lett. **119**, 243901 (2017).

[49] A. F. Sadreev and E. Y. Sherman, Phys. Rev. A **94**, 033820 (2016).